Enhanced in-plane ferroelectricity in $BaTiO_3$ thin films fabricated by aqueous chemical solution deposition

T. M. Raeder, K. Bakken, J. Glaum, M. A. Einarsrud, and T. Grande

Citation: AIP Advances **8**, 105228 (2018); doi: 10.1063/1.5059549
View online: https://doi.org/10.1063/1.5059549
View Table of Contents: http://aip.scitation.org/toc/adv/8/10
Published by the American Institute of Physics

Enhanced in-plane ferroelectricity in $BaTiO_3$ thin films fabricated by aqueous chemical solution deposition

T. M. Raeder, K. Bakken, J. Glaum, M. A. Einarsrud, and T. Grande[a]
Department of Materials Science and Engineering, NTNU Norwegian University of Science and Technology, NO-7491 Trondheim, Norway

(Received 20 September 2018; accepted 18 October 2018; published online 25 October 2018)

Ferroelectric $BaTiO_3$ is widely used in capacitors, but the low Curie temperature limits a further use of $BaTiO_3$. In this work we present an aqueous chemical solution deposition (CSD) route for $BaTiO_3$ thin films, demonstrating that organic solvents are not required for CSD. Textured $BaTiO_3$ thin films were deposited on $SrTiO_3$ substrates. The in-plane dielectric properties were investigated using interdigitated electrodes and ferroelectric switching was observed up to 160±5 °C. The increased Curie temperature is proposed to result from thermal strain due to a mismatch in thermal expansion coefficient between the film and the substrate, and is in good agreement with the theory of strain engineering in $BaTiO_3$. Finally, the decomposition and crystallization of $BaTiO_3$ during thermal treatment were determined by the combination of thermal analysis, IR spectroscopy and X-ray diffraction of powder prepared from the solution. https://doi.org/10.1063/1.5059549

I. INTRODUCTION

$BaTiO_3$ is widely used in capacitors due to its high dielectric constant, but it is also of interest for optical modulators, ferroelectric memory, as well as other devices that seek to utilize the ferroelectric properties inherent to this material.[1–4] Several of these potential applications require thin films for miniature devices. Processing of thin films via chemical solution deposition (CSD) is attractive due to its low cost, ease of fabrication and scalability. Wet chemical methods such as CSD are also versatile tools for materials research as it is easy to adjust the chemical composition of the solution in order to study the effect of chemical substitution or dopants. For these reasons several reports on CSD of $BaTiO_3$ thin films have appeared.[5–15] Common for all previous studies is the reliance on organic solvents, which are in general irritants or toxic, and are thus also costly to handle. Replacing the organic solvents with water would therefore be beneficial, but to the best of the authors knowledge no reports of $BaTiO_3$ thin films or powder fabricated by aqueous wet chemical methods have appeared in the literature so far.

Thin films of $BaTiO_3$ made by CSD are typically made with granular texture,[16] although textured films have also been reported.[5,17,18] The substrate and synthesis conditions play important roles in the formation of texture, but the choice of substrate is also influenced by the methods used to characterize the properties. Characterization is normally done by making a parallel plate capacitor from the thin film and measuring out-of-plane properties. This requires the substrate surface to be conductive. However, by using interdigitated electrodes (IDEs) on the surface of the film, the in-plane dielectric and ferroelectric properties can be determined without the need of a conducting substrate. This has been done successfully for PZT,[19,20] but to the best of the authors knowledge no reports using IDEs to characterize ferroelectric properties of $BaTiO_3$ are available. IDEs have the advantage that the capacitance and operating voltage are decoupled from the film thickness, simplifying device design,

[a]Corresponding author: grande@ntnu.no

and ferroelectric films with IDEs are of interest for piezoelectric applications in micromechanical systems (MEMS).[19,21,22] Additionally, $BaTiO_3$ thin-film devices with IDEs are of interest for tunable capacitors[23,24] and gas sensors.[25]

Here, we report for the first time an aqueous CSD route to $BaTiO_3$ thin films. The films were deposited on single-crystal $SrTiO_3$ substrates, which have a lower thermal expansion coefficient than $BaTiO_3$,[26] resulting in in-plane tensile strain in the films during cooling from the crystallization temperature. This is predicted by theory to give increased Curie temperature and a domain pattern consisting of in-plane polarization.[27] The in-plane ferroelectric properties were determined using Pt IDEs, and the ferroelectric properties, domain pattern, and the ferroelectric transition are discussed with respect to the effect of thermal strain.

II. EXPERIMENTAL

A. Material synthesis

The aqueous precursor solution used is based on a modified Pechini method.[28] First separate solutions of Ba^{2+} and Ti^{4+} complexes were prepared. The Ba-solution was made by drying $Ba(NO_3)_2$ (Sigma-Aldrich) at 200 °C. Following this, a solution of EDTA (Sigma-Aldrich) and ammonia (30 %, Sigma-Aldrich) in deionized water was prepared at 60 °C and pH ~7. The dry $Ba(NO_3)_2$ was then added to this solution. Citric acid (Sigma-Aldrich) was added as a secondary complexing agent and the solution was stirred before the pH was adjusted back to neutral. The molar ratios were 1:1:4.8:2 for $Ba(NO_3)_2$, EDTA, ammonia, and citric acid, respectively. Typical concentrations prepared were 0.3-0.5 M. The Ti-solution was made by dissolving citric acid in deionized water and adding Ti-4-isopropoxide (Sigma-Aldrich) while the solution was kept at 80 °C. The solution was stirred at 80 °C for 12 h before the pH was adjusted to 7 by addition of ammonia. The concentration of Ti in the solution was determined by thermogravimetric analysis. Typical concentrations were 0.5-0.7 M. The Ba- and Ti-solutions were mixed in stoichiometric ratios to make the final $BaTiO_3$ precursor solution. The stability of the precursor solution was >2 years for a concentration of 0.25 M.

$BaTiO_3$ thin films were deposited on (100) single-crystal $SrTiO_3$ substrates (1x1cm, Crystal-GMBH). The solution was diluted to a concentration of 0.13 M and spin-coated onto the substrates at 3000 rpm. The substrates with the films were placed in a rapid thermal processing furnace (JetFirst 200, Jipelec) for combined pyrolysis and thermal annealing. The films were heated with 100 °C/min from ambient temperature to 450 °C, with 50 °C/min up to 550 °C and 20 °C/s up to 1000 °C. The hold time at 1000 °C was 5 min. This process was repeated 8 times to prepare thicker films.

Amorphous powder for thermal analysis was prepared by drying the solutions at 120 °C, while powders for XRD and IR was prepared from solutions dried at 200 °C for 24 h. Powder dried at 200 °C was calcined at several different temperatures for 2 h with a heating rate of 200 °C/h.

B. Materials characterization

Interdigitated electrodes were patterned using a lift-off process based on ma-N 440-series photoresist (Microchem) exposed by a maskless aligner (Heidelberg MLA 150). Ti (5 nm) and Pt (20 nm) were deposited using e-beam evaporation to form the electrodes (ATC series, AJA international). The thin films with the electrodes were annealed in air at 600 °C for 2 h with a heating and cooling rate of 200 °C/h. Finally, the samples were cleaned in isopropanol using ultrasound for 2 min. A micrograph of a set of IDEs is shown in Figure 1(a), and a schematic drawing is shown in (b). The IDEs had an electrode spacing, *a,* of 7.37 μm, electrode width of 2.63 μm, and 100 fingers with 900 μm overlap.

Electrical characterization was performed on an aixXACT TF analyzer 2000 using a thin film sample holder with integrated heating element and thermometer. The maximum electric field used was 20 kV/cm, calculated by dividing the voltage by the effective electrode spacing $a' = a+4ln(2)t/\pi$ as described in Ref. 29, where a is the actual electrode spacing and t is the film thickness. The coercive field and remnant polarization, P_0, were found from where the hysteresis loop intersects the x- and y-axis in the first quadrant of the plot.

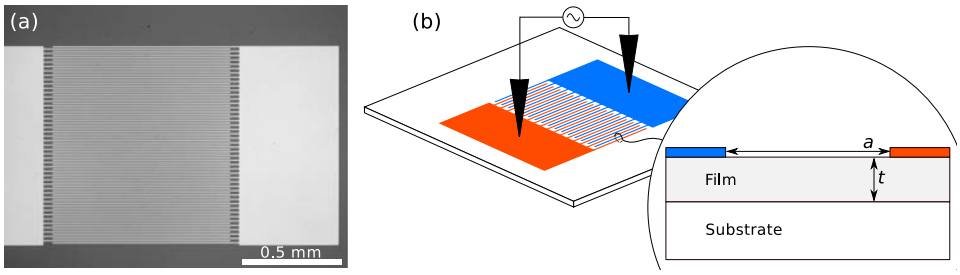

FIG. 1. (a) Electron microscope image of the IDE structure used. (b) Schematic drawing of an IDE structure. A cross-section is highlighted, with the electrode spacing a and film thickness t shown.

The thin-films were investigated by X-ray diffraction (XRD) using a PanAlytical Empyrean diffractometer with a, a 4xGe220 monochromator, and a 2D detector. Scanning electron microscopy of the thin film surface was performed on a FEI APREO field-emission SEM in immersion mode using a backscatter electron detector, while the cross section was studied using a Zeiss SUPRA 55VP field-emission SEM with an in-lens detector. Cross section of the film was obtained by fracturing the substrate into two parts.

XRD patterns of powder samples were recorded using a Bruker D8 A25 DaVinci Diffractometer. Infrared spectra of the powders from 400 to 4000 cm^{-1} were measured using a Bruker FTIR instrument (VERTEX 80v) and a Bruker Platinum ATR diamond system. 32 scans were collected and averaged for each sample with a resolution of 4 cm^{-1}. Thermal analysis and differential scanning calorimetry (DSC) was performed on a NETZSCH STA 449C simultaneous thermal analyzer by heating at 10 °C/s.

III. RESULTS

The XRD pattern of a $BaTiO_3$ thin film deposited on a (100) $SrTiO_3$ substrate is shown in Figure 2. Only (100) and (200) pseudo-cubic Bragg reflections of $BaTiO_3$ are observed, together with the reflections from the $SrTiO_3$ substrate. The absence of other reflections demonstrate that the $BaTiO_3$ thin films are phase pure and highly textured. The out-of-plane lattice parameter is found to be 4.000±0.005 Å based on the (200) reflection, which is close to the unit cell a-parameter at 3.992 Å for bulk $BaTiO_3$.

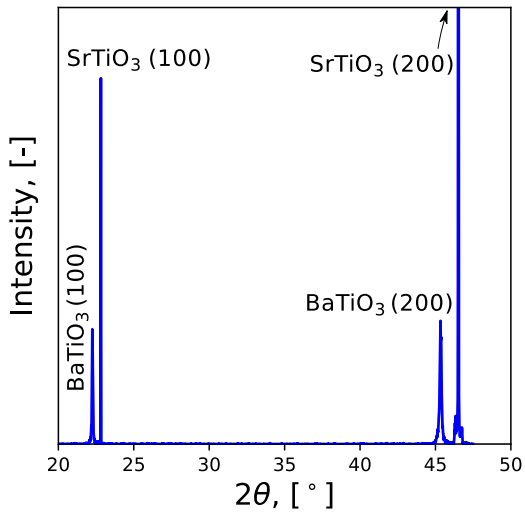

FIG. 2. Typical θ-2θ diffraction pattern of the $BaTiO_3$ thin films on (100) oriented $SrTiO_3$ showing the (100) and (200) reflections of both the substrate and the film.

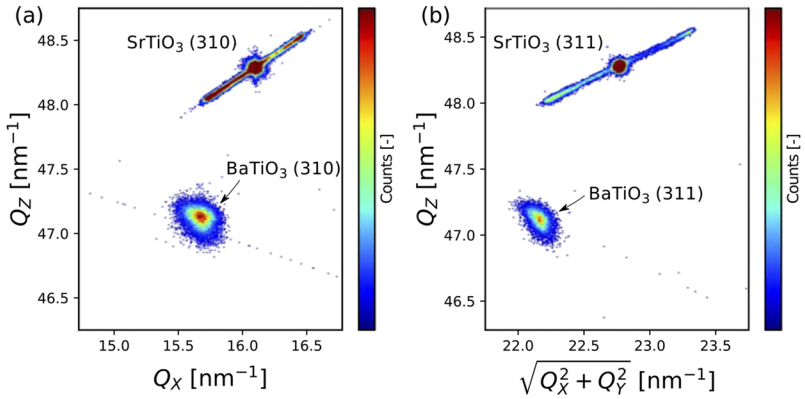

FIG. 3. Reciprocal space maps around the (a) (310) reflection and (b) (311) reflection. The lines of higher intensity through the $SrTiO_3$ reflections are an artefact from the monochromator, which can also be seen in Figure 2 at the base of the $SrTiO_3$ (200) reflection.

Reciprocal space maps around the (310) and (311) reflections are shown in Figure 3. The relation between the $SrTiO_3$ and $BaTiO_3$ reflections show that the film is epitaxial. The pseudo cubic (310) $BaTiO_3$ reflection gives an out-of-plane lattice parameter of 4.000±0.007 Å and average in-plane lattice parameter of 4.010±0.023 Å, while the pseudo cubic (311) reflection results in an out-of-plane lattice parameter of 4.000±0.007 Å and average in-plane lattice parameter of 4.010±0.013 Å. The out-of-plane lattice parameters are in good agreement with data in Figure 2, and have comparable uncertainty, significantly smaller than the uncertainty of in-plane parameters. The average in-plane lattice parameters from the (310) and (311) reflections are nearly identical, but the uncertainty is significantly larger for the (310) reflection than for the (311) reflection.

A SEM micrograph of the surface of a $BaTiO_3$ thin film is shown in Figure 4. The thickness of the film was measured to be 180±6 nm based on cross-section SEM images. A SEM image of the cross-section is shown in the inset in Figure 4.

The ferroelectric nature of the films are evident from the P-E-loop, shown in Figure 5(a). The coercive field is 5 kV/cm and the remnant polarization is 13 μC/cm^2. Figure 5(b) shows the derivative of the polarization as a function of field, where the peaks correspond to the positive and negative switching events. The full width half maximum (FWHM) of the peaks are ~ 3.4 kV/cm demonstrating

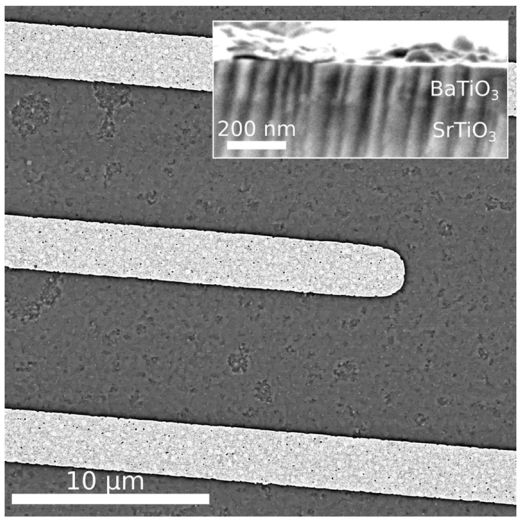

FIG. 4. SEM image of the $BaTiO_3$ film surface with the Pt IDEs. The inset shows the cross-section of the film and substrate.

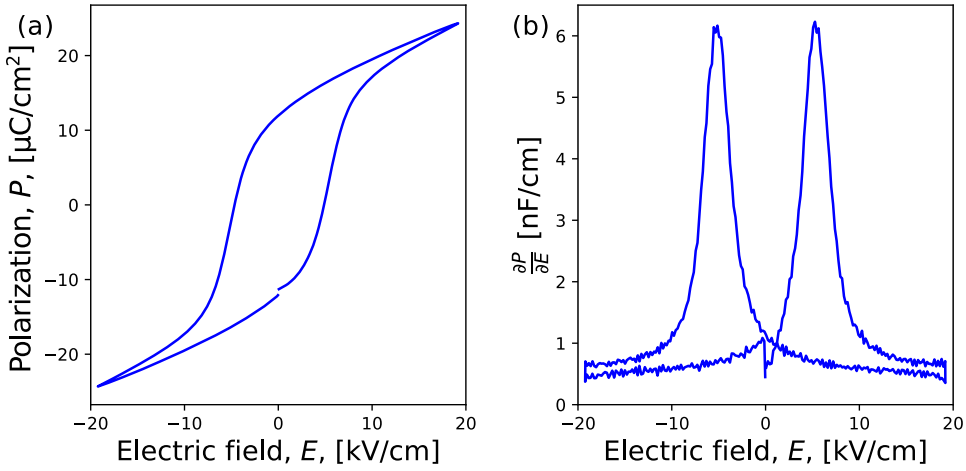

FIG. 5. (a) Hysteresis loop captured at 1 Hz and 25 °C and (b) the derivative of polarization with respect to field, calculated from the current.

sharp switching events. A sizable capacitive contribution from the substrate is also evident, recognized by the high baseline (~0.56 nF/cm) in Figure 5(b).

The temperature dependence of the ferroelectric hysteresis loop is shown in Figure 6(a). The remnant polarization and coercive field are decreasing with increasing temperature, and the remnant polarization as a function of temperature is shown in Figure 6(b). A dashed line is included showing the expected behavior of a Landau-Devonshire second order ferroelectric phase transition for an unclamped system,[30] and a good fit is observed for the lower temperature range. According to this model the remnant polarization should be zero above 126 °C, but the experimental results deviate, and the hysteresis loop in (a) recorded at 160 °C still shows signature of ferroelectric behavior. When the temperature was increased further, the leakage current become enhanced, and the polarization could not be determined accurately. Based on the experimental data the Curie temperature was estimated to be 160±5 °C.

Thermal processing of the thin films was based on the study of the thermal decomposition and crystallization of the amorphous powder, prepared from the precursor solution by drying. The thermal analysis is shown in Figure 7. No significant mass loss is observed until ~ 200 °C where the sample starts to decompose. This decomposition is endothermic in nature, as evidenced by the DSC signal.

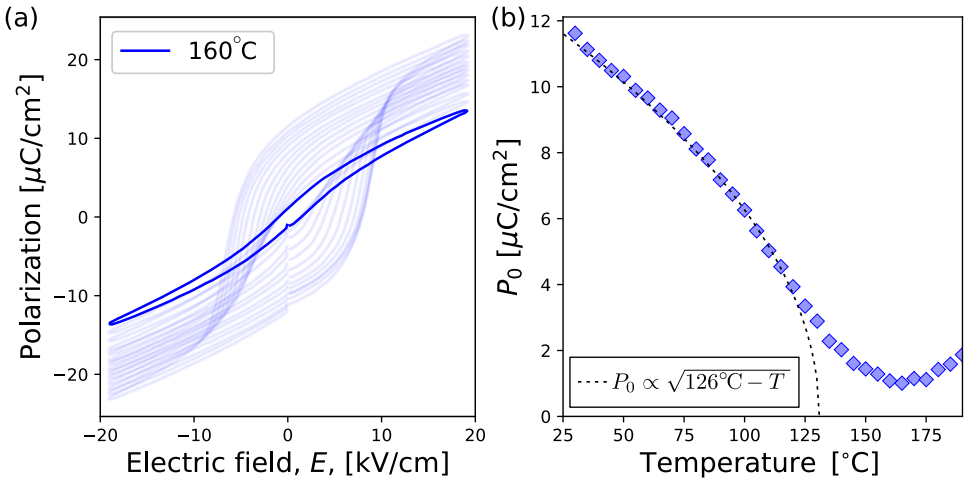

FIG. 6. (a) Temperature dependence of the P-E hysteresis loops shown for every 10 °C from 30 °C to 160 °C. 3000 Hz was used to minimize the effect of leakage and (b) temperature dependence of the remnant polarization determined from the hysteresis loops. The dashed line indicates the expected behavior of a second order phase transition in an unclamped system.

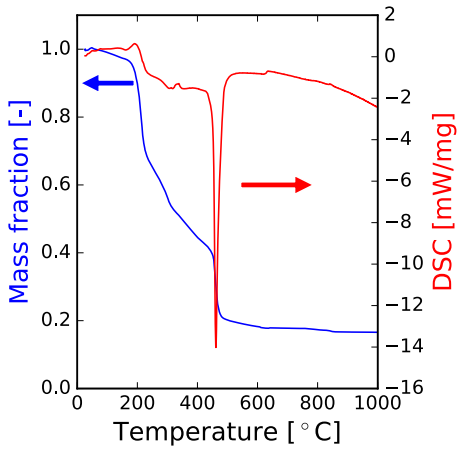

FIG. 7. Thermal analysis of the amorphous gel showing the mass loss (left) and exothermic/endothermic nature (right) of the process.

Upon further heating a continuous mass loss from exothermic reactions is observed until ~ 460 °C. At this temperature a sudden mass loss occurs, which is most likely due to combustion of organic residuals in the sample. Minor mass loss is observed up to around 600 °C, where the mass stabilizes.

XRD patterns of $BaTiO_3$ powders after thermal treatment are shown in Figure 8(a). Crystalline phases appear when the powder is heat treated at 550 °C or above. The Bragg reflections are broad at 550 °C and become sharper with increasing calcination temperature. The main reflections can be indexed to $BaTiO_3$, but some more diffuse reflections are assigned to the oxycarbonate phase previously observed.[6,31–37] These broad reflections disappear at 650 °C and above, where only $BaTiO_3$ is observed.

The infrared absorption spectra of the powders calcined at different temperatures are shown in Figure 8(b). The precursor decomposes to form $BaCO_3$ and amorphous Ti-rich compounds, similar to the findings of Ischenko *et al.*[34,35] The absorption band corresponding to asymmetric stretching of TiO_6 octahedra is observed at around 500 cm^{-1} from 550 °C and above, demonstrating the presence $BaTiO_3$.

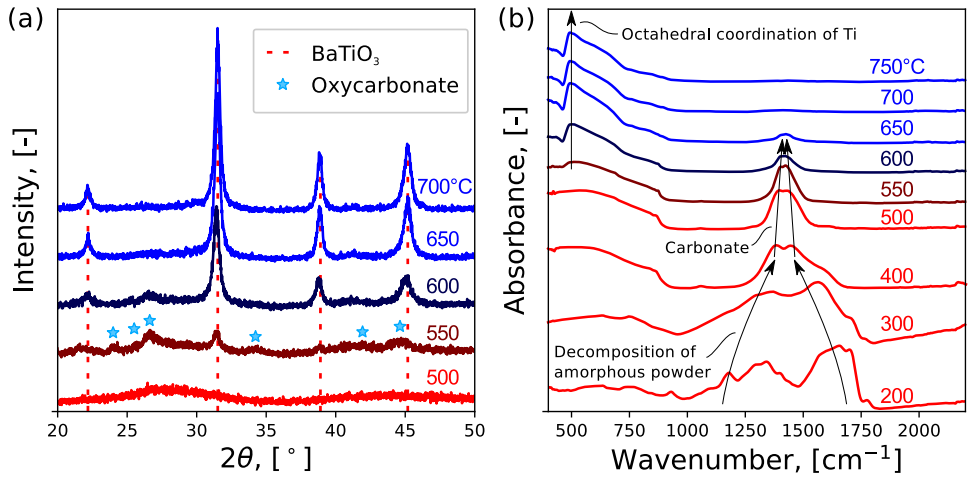

FIG. 8. (a) XRD patterns with the reflections associated with $BaTiO_3$ (ICDD PDF 01-070-9164, 2016) and an oxycarbonate phase.[32,33] (b) IR spectra of $BaTiO_3$ powders. The decomposition of the amorphous powder to barium carbonate is indicated with arrows, as is the evolution of the carbonate bands and the rise of an absorption band associated with octahedral coordination of Ti. This is the coordination Ti has in $BaTiO_3$ and the color gradient from red to blue is set to coincide with the rise of this band.

IV. DISCUSSION

The thin films are found to be strongly textured (Figure 2 and 3), demonstrating heterogeneous nucleation and growth of $BaTiO_3$ on the $SrTiO_3$ substrate. However, the thin films are not epitaxially strained, as the thickness of the films exceed by far the critical thickness for relaxation of the lattice parameter relative to the lattice parameter of the substrate. Epitaxial strain in $BaTiO_3$ thin films on $SrTiO_3$ substrate would lead to a compressive strain due to a smaller lattice parameter of $SrTiO_3$ relative to $BaTiO_3$. On the contrary, our hypothesis is that a tensile strain is developed due to thermal strain as discussed by Evans and Hutchinson.[38] The film was thermally annealed at 1000 °C which resulted in films with high crystallinity and texture and with strong adhesion to the substrate (Figure 4). Upon cooling, the substrate contracts according to the thermal expansion. The thermal expansion of $BaTiO_3$ (~ 12.8×10^{-6} K^{-1} in the range 120 to 1000 °C) is larger than that of $SrTiO_3$ (~ 11.5×10^{-6} K^{-1}) but the film is clamped to the substrate and cannot contract freely. This causes in-plane tensile strain in the film as it cools from 1000 °C to ambient temperature as illustrated in Figure 9. The in-plane tensile strain is suggested to energetically favor polarization in the in-plane direction, rather than out-of-plane.[27] The in-plane tensile strain is observed experimentally (Figure 3), where the average in-plane lattice parameter (4.010 Å) is larger than the out-of-plane lattice parameter (4.000 Å).

A high remnant polarization and sharp switching events are observed in the films when compared to other films prepared by CSD.[18,39–49] This can be explained by the use of interdigitated electrodes that measure in-plane polarization, combined with the tensile strain that stabilizes the polarization in-plane. Strain has previously been used to enhance the polarization and Curie temperature in $BaTiO_3$ by utilizing compressive epitaxial strain.[50,51] This requires deposition at low temperature to avoid relaxation, typically achieved by molecular beam epitaxy or pulsed laser deposition. The current CSD process resulting in thicker films and utilize strain induced by the mismatch in thermal expansion. The in-plane thermal strain close to T_C is estimated to 0.1 % with respect to the cubic phase. This level of strain is predicted to increase the Curie temperature to about 150 °C,[27] but the experimental results indicate a slightly higher Curie temperature (160 °C). However, it should be noted that the theoretical predictions were made by assuming a single-domain state at all temperatures with polarization in the [110] direction. Uneven strain in the film due to the thickness may also contribute to a different strain field close to the interface. The measured polarization values are approximately half of the polarization observed in $BaTiO_3$ single crystals,[52] but the coercive field is significantly higher[52] and comparable to the coercive field measured in films made by CSD with parallel plate electrodes.[18]

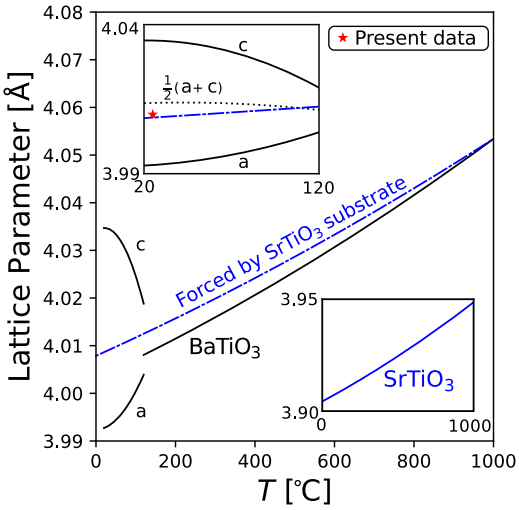

FIG. 9. Evolution of the average in-plane lattice parameter of the $BaTiO_3$ film as enforced by the substrate. The lattice parameters of bulk $BaTiO_3$ are shown for comparison. The upper inset shows a close up of the 20-120 °C range, and the average of the bulk *a* and *c* parameters is indicated by the dotted line. The experimentally observed average in-plane lattice parameter is also indicated. The lower inset shows the lattice parameter of $SrTiO_3$ as a function of temperature. Polynomial expressions for thermal expansion are taken from Ref. 26.

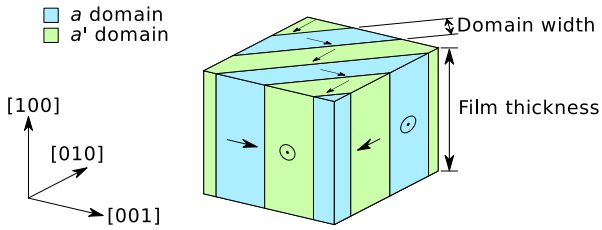

FIG. 10. Schematic illustration of the *a-a'* domain pattern suggested for the $BaTiO_3$ films. Arrows are used to indicate the polarization direction, and the lattice is elongated along the same axis.

The reciprocal space maps (Figure 3) revealed an in-plane lattice parameter that is larger than the out-of-plane lattice parameter. The in-plane lattice parameter also has a large uncertainty, and the uncertainty is larger for the data from the 310 reflection than the 311 reflection. This indicates in-plane domains and the formation of an *a-a'* domain pattern, as schematically shown in Figure 10. In this domain pattern, alternating domains have unit cells elongated in the [010] and [001] pseudo-cubic directions, and the pattern arises in order for the film to minimize stress. Since the polarization in $BaTiO_3$ follows the long axis, the domains also have alternating polarization directions, and are expected to form electrically neutral 45° domain walls as shown. The inset in Figure 9 shows the extrapolated in-plane lattice parameter of $BaTiO_3$ constrained by the thermal contraction of the $SrTiO_3$ substrate, which is in good agreement with the observed average in-plane lattice parameter.

Finally, the thermal processing of the films was developed based on the insight in the thermal decomposition and crystallization of the amorphous $BaTiO_3$ powder. An oxycarbonate phase was observed to be formed at 550 °C and vanish at 650 °C, where formation of phase pure $BaTiO_3$ was confirmed by XRD. These results indicate a similar reaction mechanism as proposed by Ischenko (Equation 1),[34] where the $BaTiO_3$ forms through the reaction between barium oxycarbonate and amorphous barium deficient barium titanate.

$$(\mathrm{Ba,\ Ti}) - \text{precursor complex} \rightarrow (1-y)\mathrm{BaO}_x(\mathrm{CO_3})_{1-x} + \mathrm{Ba}_y\mathrm{TiO}_{2+y} \rightarrow \mathrm{BaTiO_3} \quad (1)$$

V. CONCLUSION

An aqueous chemical solution route for preparation of $BaTiO_3$ powders and thin films was developed. $BaTiO_3$ was shown to form via an intermediate carbonate phase, which transformed to phase pure $BaTiO_3$ when calcined at 650 °C or above. Epitaxial thin films were grown on $SrTiO_3$ substrates at 1000 °C. The in-plane ferroelectric properties of the films were confirmed by using IDEs, and a domain pattern was suggested based on reciprocal space mapping. The ferroelectric properties are characterized by high remnant polarization and sharp switching when compared to other films made by CSD. Ferroelectric switching was also confirmed at temperatures above the Curie temperature for bulk $BaTiO_3$, demonstrating the effect of in-plane tensile strain developed due to thermal mismatch with the substrate.

ACKNOWLEDGMENTS

Financial support from NTNU and The Research Council of Norway under the Toppforsk program to the project (No 250403) "From Aqueous Solutions to oxide Thin films and hierarchical Structures" (FASTS) is gratefully acknowledged. The Research Council of Norway is also acknowledged for the support to the Norwegian Micro- and Nano-Fabrication Facility, NorFab, project number 245963/F50. Finally, we acknowledge use of the Norwegian Center for X-ray Diffraction, Scattering and Imaging (RECX).

[1] J. F. Scott, Science **315**, 954 (2007).
[2] K.-H. Chen, Y.-C. Chen, Z.-S. Chen, C.-F. Yang, and T.-C. Chang, Appl. Phys. A **89**, 533 (2007).
[3] N. Setter, D. Damjanovic, L. Eng, G. Fox, S. Gevorgian, S. Hong, A. Kingon, H. Kohlstedt, N. Y. Park, G. B. Stephenson, I. Stolitchnov, A. K. Taganstev, D. V. Taylor, T. Yamada, and S. Streiffer, J. Appl. Phys. **100**, 051606 (2006).

[4] L. Mazet, S. M. Yang, S. V. Kalinin, S. Schamm-Chardon, and C. Dubourdieu, Sci. Technol. Adv. Mater. **16**, 036005 (2015).
[5] R. W. Schwartz, P. G. Clem, J. A. Voigt, E. R. Byhoff, M. Van Stry, T. J. Headley, and N. A. Missert, J. Am. Ceram. Soc. **82**, 2359 (1999).
[6] U. Hasenkox, S. Hoffmann, and R. Waser, J. Sol-Gel Sci. Tech. **12**, 67 (1998).
[7] M. C. Gust, L. A. Momoda, N. D. Evans, and M. L. Mecartney, J. Am. Ceram. Soc. **84**, 1087 (2001).
[8] S. Halder, T. Schneller, and R. Waser, J. Sol-Gel Sci. Tech. **33**, 299 (2005).
[9] S. Hoffmann and R. Waser, J. Eur. Ceram. Soc. **19**, 1339 (1999).
[10] L. Radonjić, M. Todorović, and J. Miladinović, J. Sol-Gel Sci. Tech. **45**, 125 (2008).
[11] M. Manso-Silván, L. Fuentes-Cobas, R. J. Martín-Palma, M. Hernández-Vélez, and J. M. Martínez-Duart, Surf. Coatings Tech. **151-152**, 118 (2002).
[12] T. M. Stawski, S. A. Veldhuis, R. Besselink, H. L. Castricum, G. Portale, D. H. A. Blank, and J. E. ten Elshof, J. Phys. Chem. C **116**, 425 (2012).
[13] D. S. Paik, A. V. P. Rao, and S. Komarneni, J. Sol-Gel Sci. Tech. **10**, 213 (1997).
[14] W. Ousi-Benomar, S. S. Xue, R. A. Lessard, A. Singh, Z. L. Wu, and P. K. Kuo, J. Mater. Res. **9**, 970 (1994).
[15] M. C. Gust, N. D. Evans, L. A. Momoda, and M. L. Mecartney, J. Am. Ceram. Soc. **80**, 2828 (1997).
[16] R. W. Schwartz, T. Schneller, and R. Waser, Comptes Rendus Chimie **7**, 433 (2004).
[17] R. W. Schwartz, Chem. Mater. **9**, 2325 (1997).
[18] T. Hosokura, A. Ando, and T. Konoike, RSC Adv. **5**, 97563 (2015).
[19] N. Chidambaram, A. Mazzalai, D. Balma, and P. Muralt, IEEE Trans. Ultrason. Ferroelectr. Freq. Control **60**, 1564 (2013).
[20] N. Chidambaram, D. Balma, R. Nigon, A. Mazzalai, R. Matloub, C. S. Sandu, and P. Muralt, J. Micromech. Microeng. **25**, 045016 (2015).
[21] B. Xu, R. G. Polcawich, S. Trolier-McKinstry, Y. Ye, L. E. Cross, J. J. Bernstein, and R. Miller, Appl. Phys. Lett. **75**, 4180 (1999).
[22] E. Hong, S. V. Krishnaswamy, C. B. Freidhoff, and S. Trolier-McKinstry, Sensors Actuators, A Phys. **119**, 520 (2005).
[23] A. Khalfallaoui, L. Burgnies, K. Blary, G. Velu, D. Lippens, and J. C. Carru, IEEE Trans. Ultrason. Ferroelectr. Freq. Control **62**, 247 (2015).
[24] H. N. Al-Shareef, D. Dimos, M. V Raymond, and R. W. Schw, J. Electroceramics **1**, 145 (1997).
[25] M.-S. Lee and J.-U. Meyer, Sensors Actuators B Chem **68**, 293 (2000).
[26] D. Taylor, Trans. J. Br. Ceram. Soc. **84**, 181 (1985).
[27] N. A. Pertsev, A. G. Zembilgotov, and A. K. Tagantsev, Phys Rev. Lett. **80**, 1988 (1998).
[28] T. O. L. Sunde, T. Grande, and M.-A. Einarsrud, *Handb. Sol-Gel Sci. Tech.* (Springer International Publishing, Cham, 2016), p. 1.
[29] C. H. Nguyen, R. Nigon, T. M. Raeder, U. Hanke, E. Halvorsen, and P. Muralt, J. Phys. D. Appl. Phys. **51**, 175303 (2018).
[30] M. E. Lines and A. M. Glass, *Principles and Applications of Ferroelectrics and Related Materials* (Oxford university press, 1977) p. 372.
[31] J.-D. Tsay, T. T. Fang, T. A. Gubiotti, and J. Y. Ying, J. Mater. Sci. **33**, 3721 (1998).
[32] P. Durán, D. Gutierrez, J. Tartaj, M. A. Bañares, and C. Moure, J. Eur. Ceram. Soc. **22**, 797 (2002).
[33] S. Gablenz, H.-P. Abicht, E. Pippel, O. Lichtenberger, and J. Woltersdorf, J. Eur. Ceram. Soc. **20**, 1053 (2000).
[34] V. Ischenko, E. Pippel, R. Köferstein, H.-P. Abicht, and J. Woltersdorf, Solid State Sci. **9**, 21 (2007).
[35] V. Ischenko, J. Woltersdorf, E. Pippel, R. Köferstein, and H.-P. Abicht, Solid State Sci. **9**, 303 (2007).
[36] P. Durán, F. Capel, D. Gutierrez, J. Tartaj, M. A. Bañares, and C. Moure, J. Mater. Chem. **11**, 1828 (2001).
[37] S. Kumar, G. L. Messing, and W. B. White, J. Am. Ceram. Soc. **76**, 617 (1993).
[38] A. G. Evans and J. M. Hutchinson, Acta Metal. Mater. **43**, 2507 (1995).
[39] M. N. Kamalasanan, S. Chandra, P. C. Joshi, and A. Mansingh, Appl. Phys. Lett. **59**, 3547 (1991).
[40] E. J. H. Lee, F. M. Pontes, E. R. Leite, E. Longo, J. A. Varela, E. B. Araujo, and J. A. Eiras, J. Mater. Sci. Lett. **19**, 1457 (2000).
[41] J. Xu, J. Zhai, and X. Yao, J. Alloys Compd. **467**, 567 (2009).
[42] M. N. Kamalasanan, N. D. Kumar, and S. Chandra, J. Appl. Phys. **74**, 5679 (1993).
[43] M. Kuwabara, S. Takahashi, and T. Kuroda, Appl. Phys. Lett. **62**, 3372 (1993).
[44] T. Hayashi, N. Ohji, K. Hirohara, T. Fukunaga, and H. Maiwa, Jpn. J. Appl. Phys. **32**, 4092 (1993).
[45] T. Hayashi, N. Oji, and H. Maiwa, Jpn. J. Appl. Phys. **33**, 5277 (1994).
[46] H. B. Sharma and A. Mansingh, J. Phys. D. Appl. Phys. **31**, 1527 (1998).
[47] J.-G. Cheng, X.-J. Meng, B. Li, J. Tang, S.-L. Guo, J.-H. Chu, M. Wang, H. Wang, and Z. Wang, Appl. Phys. Lett. **75**, 2132 (1999).
[48] R. Thomas, D. C. Dube, M. N. Kamalasanan, and S. Chandra, Thin Solid Films **346**, 212 (1999).
[49] H. Basantakumar Sharma, H. N. K. Sarma, and A. Mansingh, J. Mater. Sci. **34**, 1385 (1999).
[50] K. J. Choi, M. Biegalski, Y. L. Li, A. Sharan, J. Schubert, R. Uecker, P. Reiche, Y. B. Chen, X. Q. Pan, V. Gopalan, L.-Q. Chen, D. G. Schlom, and C. B. Eom, Science **306**, 1005 (2004).
[51] S. Kobayashi, K. Inoue, T. Kato, Y. Ikuhara, and T. Yamamoto, J. Appl. Phys. **123**, 064102 (2018).
[52] A. J. Moulson and J. M. Herbert, *Electroceramics: Materials, Properties, Applications* (John Wiley & Sons, 2003) p. 78.